The Influence of Geometry on the Initiation of Turbulence in the Vocal Tract During the Production of Fricatives

Gordon Ramsay and Christine Shadle

Haskins Laboratories, 300 George Street, New Haven, CT 06511, USA

ramsay@haskins.yale.edu, shadle@haskins.yale.edu

Abstract. *This paper examines the influence of geometry on the initiation of turbulence in fricative consonants. Large-eddy simulations of three-dimensional viscous incompressible flow are used to visualize the process of turbulent jet formation in an elliptical duct with a constriction, representing the vocal tract. Using two different geometries, the effect of asymmetry in the constriction, asymmetry in the duct shape, and proximity of the constriction to the duct walls are investigated. Results indicate that all of these factors significantly affect the vorticity field, and are likely to influence aeroacoustic source generation.*

1. Introduction

Understanding the physical mechanisms underlying the generation of turbulent sound sources during speech is important, since many speech sounds are characterized by properties of those sources. At present, we do not fully understand the many factors that may potentially influence the production of turbulence in the vocal tract. In this paper, we examine the influence of vocal tract geometry on the initiation of turbulence in fricatives.

It has long been recognized that the small area of the constriction is necessary to produce the turbulence essential to fricatives. Mechanical modelling studies have shown that the *shape* of the constriction and of the cavities downstream of the constriction can also have a significant effect on the sound produced, but models used by speech researchers have only gradually incorporated this knowledge. Meyer-Eppler (1953) used elliptical as well as circular constrictions in his early work, but he is most often cited for determining the critical Reynolds number appropriate for fricatives. Heinz (1958) used a circular constriction inside a duct in a spherical baffle, and advocated detailed measurement of the flow field to determine source distribution, but though spectra resulting from circular jets have been used for fricative noise sources, they have typically been modelled as localized and the location determined heuristically (Fant, 1970). The effect of the duct on the sound power of a turbulent source, established by Heller and Widnall, was used by Stevens (1971), but the spectral shape he used was that of a free jet.

Shadle (1985) showed that an obstacle in the path of a jet did result in strong, localized sound generation, and it was possible experimentally to measure the source independently of its location in the duct. While the obstacle source was shown to model the role of the teeth in sibilants, for non-sibilants a wall source was needed, produced by using a non-circular constriction flush with the duct wall. Experimentally it was not possible to assess the wall source properties independently of its role as a part of the

duct, beyond demonstrating that sound generation was distributed over some distance beginning at the constriction exit (Shadle, 1991).

It is clear from vocal tract imaging studies of fricatives (Subtelny et al., 1972; Narayanan et al., 1995) that the constriction shape, palate shape in and downstream of the constriction, distance to the teeth and their positions, all vary between fricatives and across subjects. Results in the fluid mechanics literature show that related parameters such as nozzle shape and the shape of the region downstream of the nozzle affect the initiation of turbulence, the flow separation point, and the structure of the turbulent flow field (e.g. Hussain and Husain, 1989). These hydrodynamic properties are more difficult to observe experimentally than the acoustic field, but we need to know more about them to be able to understand how to characterize vocal tract geometric factors that matter in turbulent sound generation.

Numerical simulation of the flow offers one way to study such properties, but there are different severe constraints. Recently, turbulent flow simulations have begun to be feasible for investigating fricative-like geometries, but are still limited in resolution. Some recent work done on glottal jets shows useful ways of using simulation and indicates effects worth investigating for fricatives. Pelorson et al. (1997) have compared flow visualization to simulation results to arrive at a model of the point of flow separation, and to study initiation of turbulence in the glottal jet and for bilabials. Researchers at Purdue University have combined mechanical models, aeroacoustic theory, and numerical models to establish the strengths of different types of aeroacoustic sources at the glottis and study of the effects of confining the glottal jet (Zhang et al., 2004; Suh, 2006).

A number of recent studies have attempted to integrate these different approaches into aeroacoustic models of fricatives. Krane (2005) approximated the process of turbulent formation based on a caricature of a free circular jet. Howe and McGowan (2005) made no assumptions about jet structure, but developed a theoretical model of interaction between a confined region of turbulence and the acoustic field to model /s/ production. Nozaki (2005) and Adachi et al. (2005) both used highly realistic geometries of the constriction and teeth, and focused on predicting the radiated sound; they did not attempt to determine the effect of specific geometric parameters. In this paper we discuss an approach using simpler model shapes and investigating the hydrodynamic field, with the goal of figuring out which geometric parameters are most important to model.

2. Turbulent Flow in Free and Confined Jets

Turbulence is generated in ducts when an initially laminar flow breaks down under the influence of shear stresses and non-linear convection, such that energy in large-scale coherent flow structures cascades down to smaller length scales, where it is dissipated by the action of viscous forces. A small portion of the unsteady turbulent energy in the hydrodynamic flow field is converted into sound, acting as an equivalent aeroacoustic source distribution that excites the acoustic eigenmodes of the duct to create small isentropic compressible flow perturbations that propagate into the far field as sound waves.

In fricatives, turbulence arises when the boundary layer formed along the wall of a tight constriction separates from the wall at the exit of the constriction. The resulting free shear layer is convected downstream by the mean flow, and rolls up into a succession

of vortical structures that eventually break down into turbulence. The laminar core of the flow exiting the constriction, the conical vortex sheet bounding the core, and the turbulent mixing region outside the core together form a jet in the front cavity that may interact further with the cavity walls and the teeth.

If the constriction is circular, and vents into free space, the characteristics of the resulting jet are well known and can be determined from a small number of dimensionless scaling parameters. The behaviour of confined jets in non-circular geometries is substantially more complicated. In a free circular jet, for example, an initial primary vortex ring is followed by secondary vortices that are shed regularly through the Kelvin-Helmholtz instability in the plane perpendicular to the jet axis, and convect along the axis at half the mean flow speed. In elliptical jets, however, the cross-section of the jet expands and contracts periodically along the major and minor axes, and the vortex rings bend back and forth along the axis, breaking down into turbulence through a richer class of flow instabilities. Further complications arise when the jet approaches a rigid wall, since recirculation regions will develop that may affect the stability of the jet and the transition to turbulence.

In order to determine the implications of these effects for sound generation in fricatives, we carried out a series of numerical simulation experiments to examine turbulent jet formation in a duct with a constriction. We investigated the effect of asymmetry in the constriction, asymmetry in the duct shape, and proximity of the constriction to the duct walls. Our aim was to determine the extent to which the vorticity field in confined non-circular geometries resembles the vorticity field predicted for a circular free jet.

3. Numerical Simulations

All of our numerical simulations were carried out using STAR-CD, a commercial software package for computational fluid dynamics marketed by CD-adapco. STAR-CD is based on a finite-volume discretization of the Navier-Stokes equations, applied to a general unstructured mesh. Here we used STAR-CD to investigate the effect of changes in geometry on the initiation of turbulent flow in a simple duct representing the vocal tract.

Simulations were implemented using two geometries: (a) an elliptical constriction in an elliptical duct, with the constriction centred on the duct axis, to test the effect of radial asymmetry in the constriction and the front cavity (Figure 1); and (b) the same duct and constriction, with the constriction offset from the duct axis so that the upper wall of the constriction was flush with the upper walls of the front and back cavities, to test the effect of axial asymmetry along the duct (Figure 4). Each geometry was composed of three tube sections of constant cross-sectional area, 1cm in length, representing the back cavity, constriction, and front cavity, connected by two intermediate tube sections of variable cross-sectional area, 0.5cm in length. All of the tubes had elliptical cross-sections, with the major axis twice the length of the minor axis. The cross-sectional area of the front and back tubes was 1.25cm^2; that of the constriction was 0.125cm^2. The radius of each connecting tube varied sinusoidally along the axis to interpolate smoothly between adjacent tubes. The end of the front cavity was set in the centre of a plane circular baffle 5cm^2 in area, which was extended into a hemispherical buffer zone covering the duct exit. All of these parameters were chosen to be representative of published data for fricative geometries (e.g. Narayanan et al., 1995).

Meshing of each geometry was carried out using the automatic gridding tools provided by STAR-CD. Finer meshing is needed next to wall surfaces to capture boundary layer effects, whereas a coarser mesh can be used in the body of the fluid. A 5mm outer wall layer of hexahedral cells, 20 cells thick, was fitted to the duct wall, with cell thickness 0.05mm in the layer closest to the wall, increasing geometrically to the thickness of the uniform inner layer mesh used to fill the rest of the solution domain; this was composed of trimmed hexahedral cells defined on a Cartesian grid, with cell dimension 0.15mm. The total number of cells was 3,283,600 in the first geometry, and 3,311,000 in the second.

To model the flow, we used the Large-Eddy Simulation for viscous incompressible isothermal flow implemented in STAR-CD, based on a Smagorinsky eddy-viscosity subgrid-scale model, with the filter width derived automatically from the mesh size. Boundary conditions were defined by specifying a constant static pressure of 1kPa at the duct entrance (equivalent to 10cmH_2O behind the constriction), and a constant mass flow rate of 0.0004kg/s over the buffer zone surface (equivalent to a volume velocity of 332cm^3/s); based on the minimum constriction dimension, this implies a Reynolds number of around 5000. The duct walls and baffle surface were taken to be impermeable, with a no-slip condition at the walls. The air in the duct was taken to be initially at rest at 20°C.

To solve the flow equations, we used the numerical solver provided by STAR-CD, which is based on the PISO algorithm. Preliminary experiments were carried out to determine a suitable discretization strategy. Based on our pilot studies, a second-order Crank-Nicholson scheme was chosen for the temporal discretization, and a monotone advection and reconstruction scheme with a compression level of 0.95 was used for the spatial discretization. A time step of 1μs was found to ensure that the Courant number across the grid was less than unity for both geometries, guaranteeing numerical stability. Using the solver, solutions for the pressure and particle velocity fields were obtained numerically over an interval of 2ms for each of the two grids. Each simulation was implemented on a 16-node Opteron cluster running Linux/MPI, and took about 14 days to compute.

4. Simulation Results

Figures 2 and 3 show results for the geometry shown in Figure 1. Snapshots of the vorticity field at 0.75ms and 1.5ms respectively are shown in two cross-sections through the centre of the constriction along the major and minor axes of the duct. At 0.75ms, flow separation has occurred at the constriction exit, and an elliptically-shaped shear layer is beginning to roll up into the leading vortex ring, which is further downstream in the plane of the major axis. The jet converges along the major axis, and diverges along the minor axis, reflecting out-of-plane oscillations that are typical of elliptical (but not circular) jets. At 1.5ms, primary and secondary vortex rings can be seen in both planes convecting forward and breaking down under the influence of turbulent diffusion. In the plane of the major axis, the flow resembles a free jet, with little evidence of wall interaction. In the plane of the minor axis, however, there is strong recirculation due to the proximity of the wall, and vortex motion breaks down more rapidly, leading to a broad region of turbulent flow bounded by the shear layer and the wall. Asymmetry in the shape of the constriction is therefore reflected in asymmetries in the way the shape of the jet core develops, whereas asymmetry in the front cavity shape affects the development and stability of the turbulent mixing region along each axis.

Figures 5 and 6 show results for the geometry illustrated in Figure 4 at 0.75ms and 1.5ms respectively. This time, the flow separates around the lower edge of the constriction, but the boundary layer remains attached to the upper wall surface. An elliptical jet core develops, but does not narrow substantially due to the presence of the wall. The primary vortex ring forms, but there is only minor evidence of circulation within the boundary layer. The stability of the boundary layer attached to the wall appears to inhibit the formation of secondary vortices, which are much weaker in this geometry. Eventually, the boundary layer becomes turbulent, and a mixing region develops around the jet as before. However, the upper region of the jet in proximity to the wall does not develop the instabilities typical of a circular or elliptical free jet, and the lower region of the jet does not appear to roll up completely into the vortex structures seen in a free jet, but oscillates loosely in space. Asymmetry along the duct axis clearly affects the structure of the flow.

5. Conclusions

Current aeroacoustic analogies for fricatives rely on highly simplified descriptions of vortex dynamics within the vocal tract, largely derived from caricatures of free circular jets. Our simulation results suggest that turbulence generation in fricative geometries may be considerably more complex than these models suppose.

The shape of the jet depends on the shape of the constriction, and this affects the way the jet cross-section develops in space and time. In circular free jets, the primary vortex ring and subsequent secondary vortices are shed regularly and propagate uniformly, with a well-defined conical jet boundary and mixing layer. In elliptical free jets, however, the jet cross-section oscillates between the major axis and the minor axis, and vortices bend back and forth along the axis of the jet core.

The distance between the jet and the surface of the vocal tract is also an important factor. When the jet is confined due to proximity of the front cavity walls, strong recirculation regions develop between the jet boundary and the wall which break down vortices and speed the transition to turbulent flow; this can happen asymmetrically, and the jet may exhibit free-jet behaviour in one dimension and confined-jet behaviour in the other, if the walls of the vocal tract are closer in one direction than the other. In the extreme case where the jet grazes the wall of the front cavity, the boundary layer remains partially attached to the wall, and this stabilizes the jet core; secondary vortex shedding is reduced, and the free boundary of the jet forms an oscillating vortex sheet.

In each of these cases, the spatio-temporal vorticity distribution is quite different. Since aeroacoustic sources are determined by the unsteady vorticity field, sound source generation can therefore be expected to be strongly affected by simple changes in geometry. Despite these complexities, however, the qualitative effect of geometry on the development of the jet is quite intuitive. It should therefore be possible to use these results to develop simplified aeroacoustic models of turbulence in fricatives as a function of a small number of geometric parameters. This will form the basis for our future research.

Acknowledgement

This research was supported by NIH/NIDCD Grant DC06705 to Haskins Laboratories.

References

Adachi, S., Tanabe, Y., and Honda, K. Numerical simulation of fricative sound sources. In *Conference on Turbulences, ZAS, Berlin, Germany, 13-14 October*, 2005.

Fant, G. *Acoustic Theory of Speech Production*. Mouton, The Hague, 2nd edition, 1970.

Heinz, J. M. *Sound generation by turbulent flow in an acoustic resonator*. S.M. thesis, Department of Electrical Engineering and Computer Science, M.I.T., 1958.

Hirschberg, A. Some fluid dynamic aspects of speech. *Bulletin de la Communication Parlée*, 2:7–30, 1992.

Hixon, T. Turbulent noise sources in speech. *Folia Phon.*, 18:168–182, 1966.

Howe, M. S. and McGowan, R. S. Aeroacoustics of [s]. *Proc. R. Soc. A*, 461:1005–1028, 2005.

Hussain, F. and Husain, H. S. Elliptic jets. Part 1. Characteristics of unexcited and excited jets. *J. Fluid Mech.*, 208:257–320, 1989.

Krane, M. H. Aeroacoustic production of low-frequency unvoiced speech sounds. *J. Acoust. Soc. Am.*, 118(1):410–427, 2005.

Meyer-Eppler, W. Zum Erzeugungsmechanismus der Geräuschlaute. *Z. Phonetik*, 7(3/4): 196–212, 1953.

Narayanan, S. S., Alwan, A. A., and Haker, K. An articulatory study of fricative consonants using magnetic resonance imaging. *J. Acoust. Soc. Am.*, 98(3):1325–1347, 1995.

Nozaki, K. Numerical simulations of the sibilant [s]. In *Conference on Turbulences, ZAS, Berlin, Germany, 13-14 October*, 2005.

Pelorson, X., Hofmans, G. C. J., Ranucci, M., and Bosch, R. C. M. On the fluid mechanics of bilabial plosives. *Speech Commun.*, 22:155–172, 1997.

Shadle, C. H. *The acoustics of fricative consonants*. Ph.D. thesis, Department of Electrical Engineering and Computer Science, M.I.T., 1985.

Shadle, C. H. The effect of geometry on source mechanisms of fricative consonants. *J. Phon.*, 19:409–424, 1991.

Stevens, K. N. Airflow and turbulence considerations for fricative and stop consonants: static considerations. *J. Acoust. Soc. Am.*, 50(4):1180–1192, 1971.

Subtelny, J. D., Oya, N., and Subtelny, J. D. Cineradiographic study of sibilants. *Folia Phon.*, 24:30–50, 1972.

Suh, J. S. *Large eddy simulation of confined turbulent flows for aeroacoustics with application to phonation*. Ph.D. thesis, Purdue University, 2006.

Zhang, Z., Mongeau, L., Frankel, S. H., Thomson, S. B., and Park, J. B. Sound generation by steady flow through glottis-shaped orifices. *J. Acoust. Soc. Am.*, 116:1720–1728, 2004.

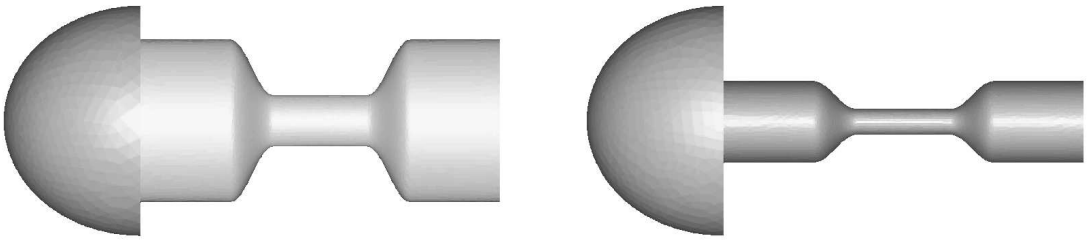

(a) major axis (b) minor axis

Figure 1: Geometry of elliptical duct with centred constriction.

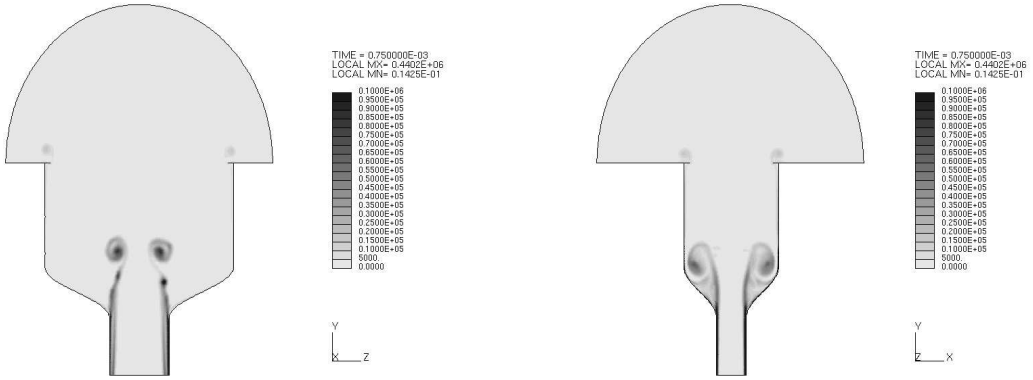

(a) major axis (b) minor axis

Figure 2: Snapshot of vorticity field at 0.75ms, showing primary vortex.

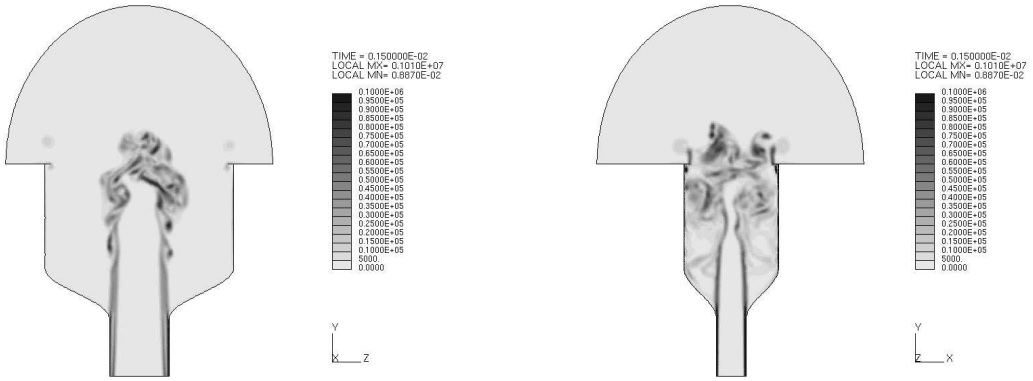

(a) major axis (b) minor axis

Figure 3: Snapshot of vorticity field at 1.5ms, showing development of secondary vortices and formation of turbulent mixing region.

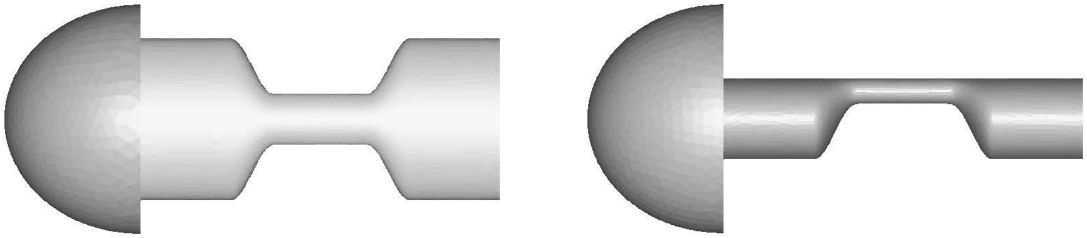

(a) major axis (b) minor axis

Figure 4: Geometry of elliptical duct with offset constriction.

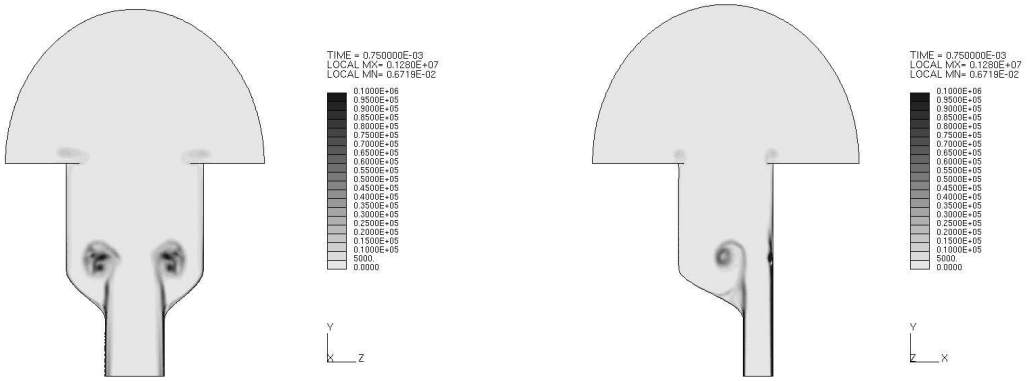

(a) major axis (b) minor axis

Figure 5: Snapshot of vorticity field at 0.75ms, showing primary vortex.

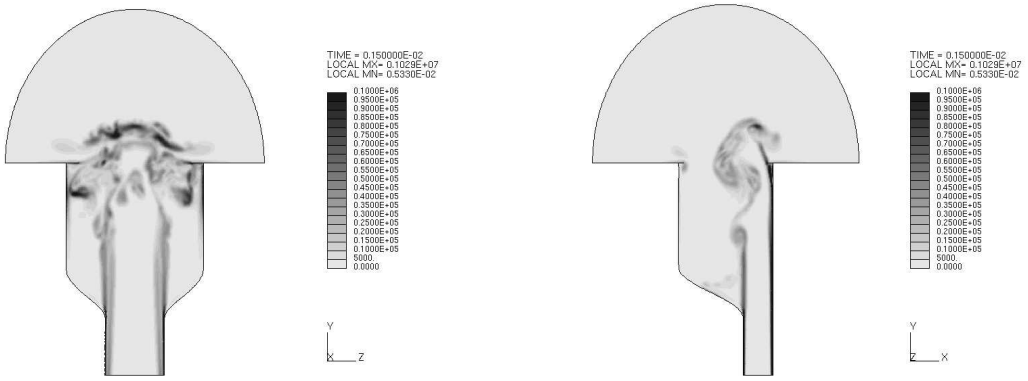

(a) major axis (b) minor axis

Figure 6: Snapshot of vorticity field at 1.5ms, showing development of secondary vortices and formation of turbulent mixing region.